Supplementary Information (SI) for Materials Horizons.
This journal is © The Royal Society of Chemistry 2025

Supporting Information

Ultraviolet durable and recyclable radiative cooling covering for efficient building energy savings

Shanshan Song[a], Congyu Hou[b], An Yang[a], Lishi Wei[a], Hongzhi Liu[a], Di Xie[a], Yongming Song[a, *]

[a]Key Laboratory of Bio-based Material Science and Technology (Ministry of Education), Northeast Forestry University, Harbin, Heilongjiang 150040, PR China

[b]State Key Laboratory of Environmental Criteria and Risk Assessment, Chinese Research Academy of Environmental Sciences, Beijing 100012, PR China

*Corresponding author

E-mail address: ymsong@nefu.edu.cn

1. Calculation and simulation

1.1 Solar reflectivity

The solar reflectivity ($\bar{R}_{solar}$) is calculated according to the following equation (S1):

$$\bar{R}_{solar} = \frac{\int_{0.25}^{2.5} I_{solar}(\lambda) R(\lambda) d\lambda}{\int_{0.25}^{2.5} R(\lambda) d\lambda} \quad \text{(S1)}$$

where the $I_{solar}(\lambda)$ is the ASTM G173 Global solar intensity spectrum and $R(\lambda)$ is the reflectivity at a specific wavelength.

1.2 Infrared emissivity

Emissivity, which is defined as the ratio of emissive energy between the object and blackbody, is utilized to characterize the objects' ability of emitting energy. The value of emissivity (ε) is calculated according to the following equations (S2-S5):

$$A(\lambda) = 1 - R(\lambda) - T(\lambda) \quad \text{(S2)}$$

$$\varepsilon(\lambda) = A(\lambda) \quad \text{(S3)}$$

$$B_{(\lambda)} = \frac{c_1 \lambda^{-5}}{exp[c_2/\lambda T)] - 1} \quad \text{(S4)}$$

$$\varepsilon = \frac{\int_{\lambda min}^{\lambda max} \varepsilon(\lambda) B(\lambda) d\lambda}{\int_{\lambda min}^{\lambda max} B(\lambda) d\lambda} \quad \text{(S5)}$$

where λ is the wavelength, $A(\lambda)$, $R(\lambda)$, $T(\lambda)$, and $\varepsilon(\lambda)$ are absorptivity, reflectivity, transmittance, and emissivity of objects at a specific wavelength, respectively. $B(\lambda)$ is the emissive energy of blackbody at a specific wavelength, c_1 is the first radiation constant (3.7418×10^8 W·μm^4 /m^2), c_2 is the second radiation constant (1.4388×10^4 μm·K), and T is the temperature.

1.3 Radiative cooling capacity

To investigate the radiative cooling performance of films in Harbin, China (45°42’52’’N, 126°38’3’’E, Altitude 150.7 m), a home-made device fabricated by an aluminum foil-coated polystyrene foam box. Four identical rectangular cavities (6 cm×8 cm×3 cm) were dug above the polystyrene foam. The films with K-type thermocouple temperature sensors were placed on the bottom of cavities. A polyethylene film was employed to seal the device to reduce the impact of convective heat generated by wind. The real-time temperature was recorded by multichannel thermoelectric coupling thermometer (Guangdong DagaSensor Technology Co., Ltd, China). The solar radiation was measured by a solar power meter (TES 1333R, TES Electrical Electronic corp., China). The ambient wind speed and humidity were recorded using an integrated portable environmental meter (EMC-9400SD, Taiwan Lutron electronic Enterprise Co., Ltd, China). The device was placed on a table to minimize the influence of heat convection from the ground.

When the radiative cooler is placed in the practical environments, the net cooling power can be expressed as follows:

$$P_{net} = P_{rad} - P_{atm} - P_{sol} - P_{cond+conv} \quad (S6)$$

Where P_{net} is the net cooling power, P_{rad} is the thermal radiative power emitted by the radiative cooler, P_{atm} is the power absorbed from atmospheric thermal radiation, P_{sol} is the absorbed incident solar radiation, $P_{(cond+conv)}$ is the heat conduction-convection from ambient radiation.

The thermal radiative power emitted by the radiative cooler is related to the surface temperature and emissivity:

$$P_{rad}(T_s) = \int cos\theta d\Omega \int_0^{\infty} I_{bb}(T_s,\lambda)\varepsilon(\lambda,\theta)d\lambda \quad (S7)$$

Where T_s is the radiative temperature of radiative cooler, θ is the local zenith angle, $I_{bb}(T_s,\lambda)$ is the spectral radiance intensity of blackbody at the temperature of T_s, $\varepsilon(\lambda,\theta)$ is the emissivity of material at the specific wavelength λ.

According to Planck's law, $I_{bb}(T_s,\lambda)$ can be expressed as:

$$I_{bb}(T_s,\lambda) = \frac{2hc^2}{\lambda^5(e^{hc/\lambda kT_s} - 1)} \quad \text{(S8)}$$

Here, h is Planck's constant, k is Boltzmann's constant, c is the speed of light.

The absorbed power of atmospheric thermal radiation by the surface of radiative cooler can be expressed as:

$$P_{atm}(T_{amb}) = \int cos\theta d\Omega \int_0^\infty I_{bb}(T_{amb},\lambda)\varepsilon(\lambda,\theta)\varepsilon_{atm}(\lambda,\theta)d\lambda \quad \text{(S9)}$$

Where T_{amb} is the ambient temperature, $\varepsilon_{atm}(\lambda,\theta)$ is the atmospheric emissivity at zenith angle θ and wavelength λ.

The absorbed incident solar radiation is can be expressed as:

$$P_{sol} = Acos\theta_{sol}\int_0^\infty I_{AM1.5}(\lambda)\varepsilon(\lambda,\theta_{sol})d\lambda \quad \text{(S10)}$$

Where θ_{sol} is the incident angle of sunlight, $\varepsilon(\lambda,\theta_{sol})$ is a function that describes the variation of the spectral emissivity of the radiative cooler, $I_{AM1.5}(\lambda)$ is the distribution intensity of the standard air mass 1.5 (AM1.5) solar spectrum.

Heat conduction-convection from ambient radiation ($P_{cond+conv}$):

$$P_{cond+conv}(T,T_{amb}) = h_{cc}(T_{amb} - T) \quad \text{(S11)}$$

Here, h_{cc} is the total conductivity coefficient between radiative cooler and surrounding environment. In the theoretical calculation, the h_{cc} was set as 3, 6, 9, 12, and 15 W m^{-2} K^{-1}, respectively.

1.4 Infrared image

The infrared images captured by infrared camera (TI450, Fluke) obeys the Stephen-Boltzmann law:

$$M_C = \varepsilon_C\sigma T_a^4 = \varepsilon_s\sigma T_b^4 + R_s\sigma T_{amb}^4 \quad \text{(S12)}$$

Where M_C is the emissive energy, ε_C is the emissivity settled by an infrared camera, ε_s

is the emissivity of target object, σ is Stephen-Boltzmann constant [σ=5.67×10^{-8} W/(m^2·K^4)], T_a is the apparent temperature displayed on the infrared camera, T_b is the practical temperature of object, T_{amb} is the ambient temperature, and R_s is the reflectivity of object.

1.5 FDTD stimulation

To simulate the scattering efficiency of the porous SEBS films with different pore size, finite-difference-time-domian (FDTD) numerical simulation was employed using perfect matching layer (PML) absorption boundary conditions and a total field scattering field (TFSF) source.

1.6 Buiding energy consumption

To calculate the annual cooling consumption of the building with baseline roofs and covered with SEBS-EC film, a building model was established in EnergyPlus 8.0. The baseline building models were installed with the conventional building materials. The dimension of building was 16 m (length) × 9 m (width) ×5.77 m (height), and the window-to wall ratio was 33%. The pitched roof features a tilt angle of 30°, with a surface area of 177.28 m^2. The cooling energy of the SEBS-EC film (the solar reflectance of 0.94, the emissivity of 0.95) was compared with that of baseline roofs in a building model. All weather data come from the official website of EnergyPlus.

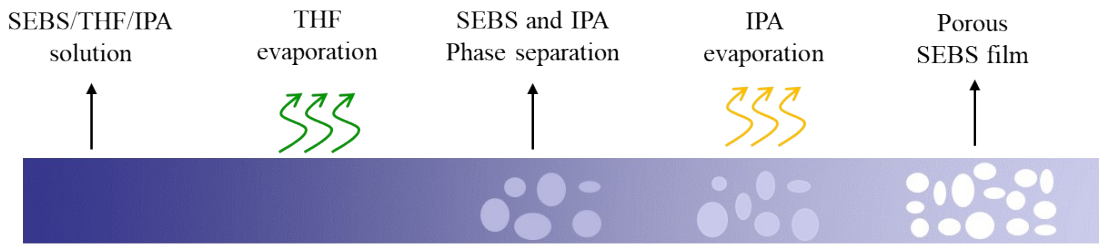

Figure S1 Schematic illustration of the fabrication process of porous SEBS film.

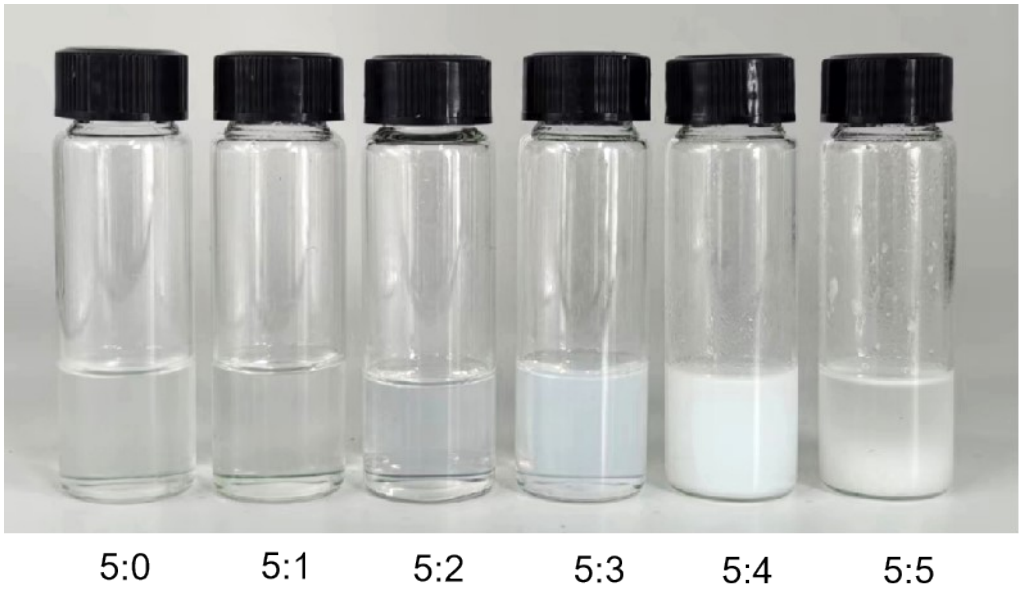

Figure S2 Photograph of SEBS/THF/IPA solutions with different volume ratios of THF and IPA.

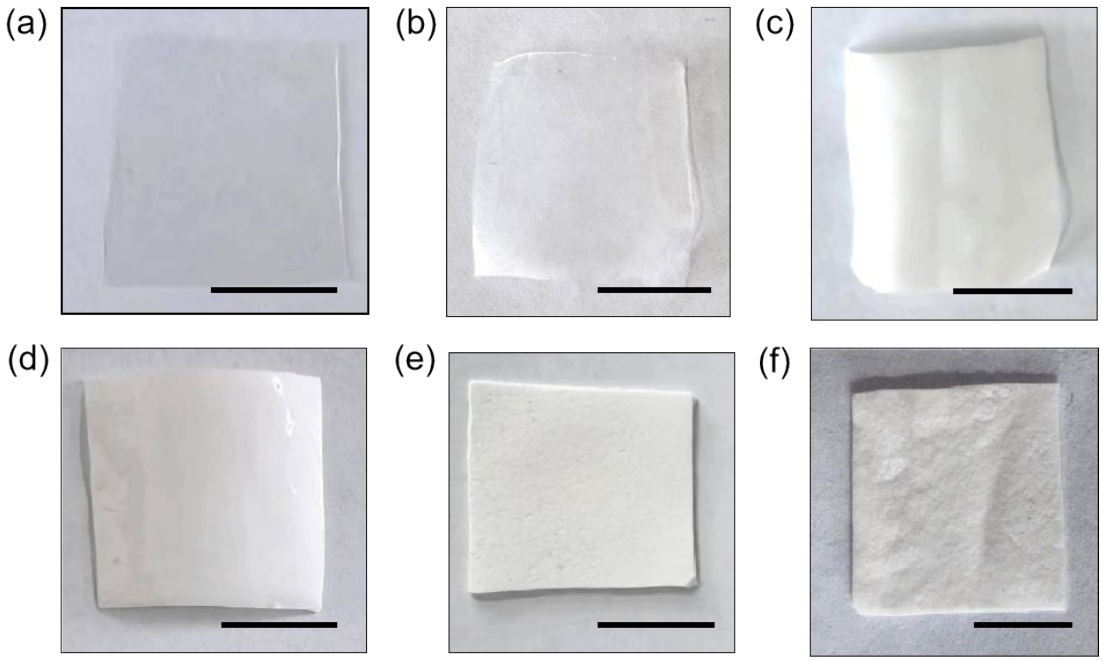

Figure S3 Photographs of (a) SEBS-0, (b) SEBS-1, (c) SEBS-2, (d) SEBS-3, (e) SEBS-4, and (f) SEBS-5 films (scale bar: 1 cm).

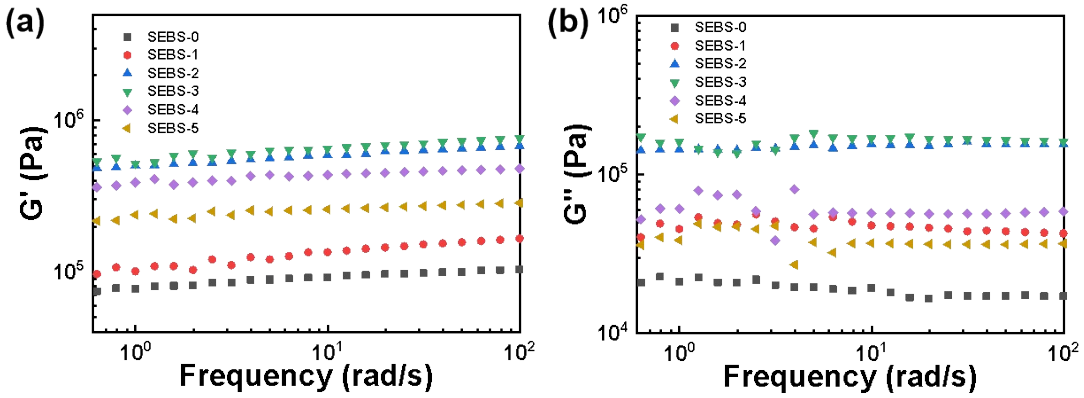

Figure S4 Storage modulus (G') and loss modulus (G'') of SEBS-0, SEBS-1, SEBS-2, SEBS-3, SEBS-4, and SEBS-5 films.

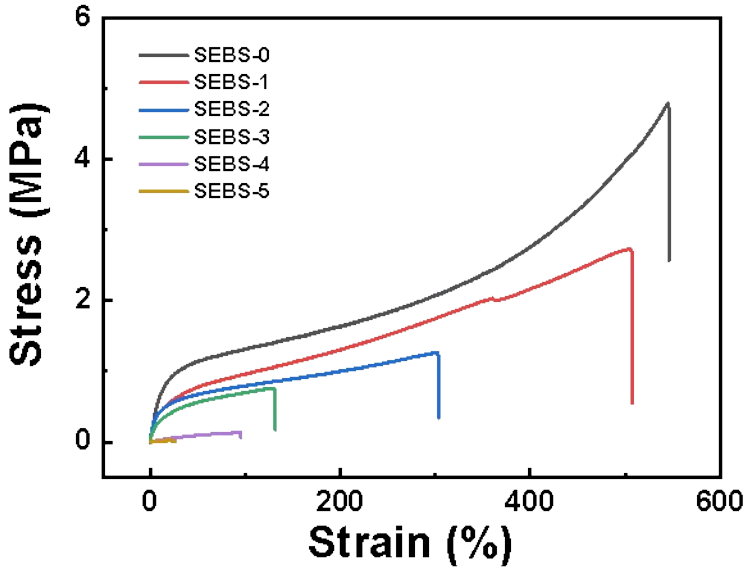

Figure S5 Strain-stress curves of SEBS-0, SEBS-1, SEBS-2, SEBS-3, SEBS-4, and SEBS-5 films.

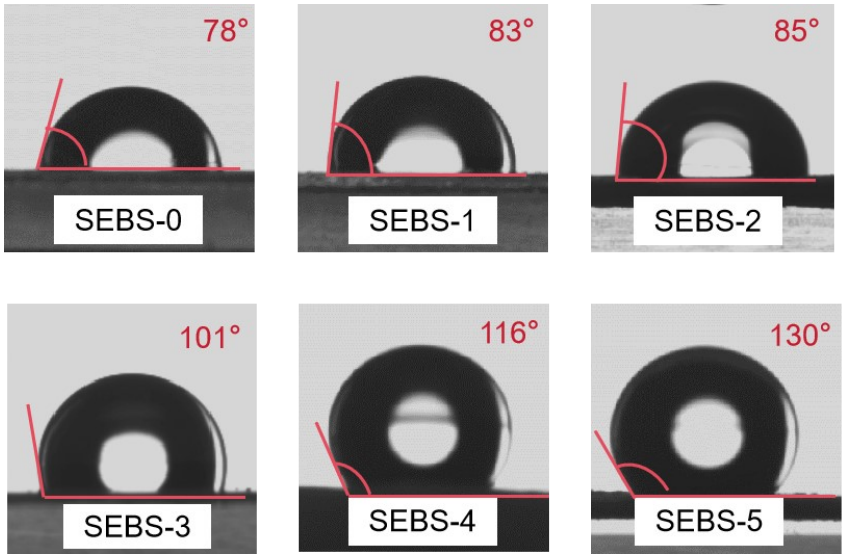

Figure S6 Water contact angles of SEBS-0, SEBS-1, SEBS-2, SEBS-3, SEBS-4, and SEBS-5 films.

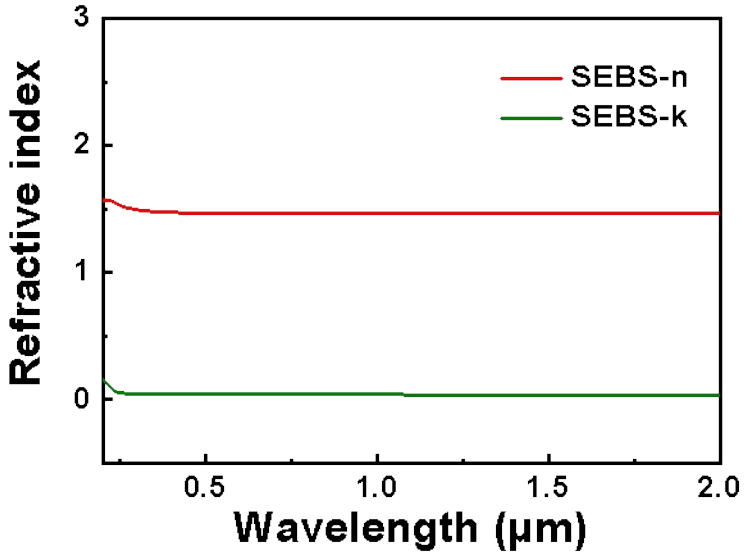

Figure S7 Optical constants of SEBS including refractive index and extinction coefficient.

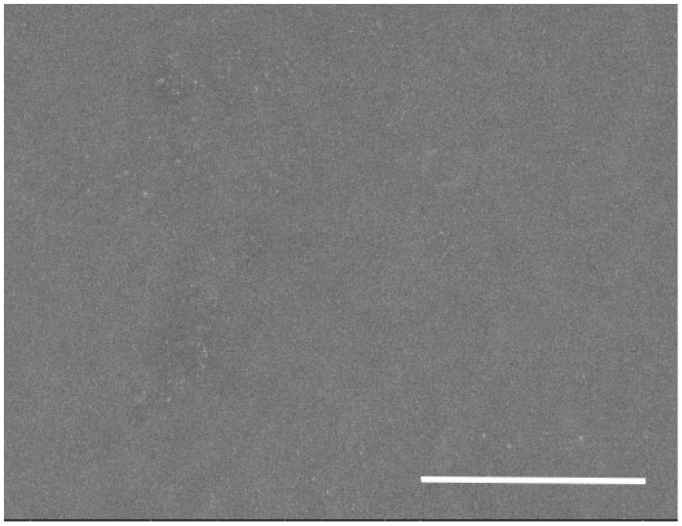

Figure S8 SEM image of SEBS-0 film (scale bar: 3 μm).

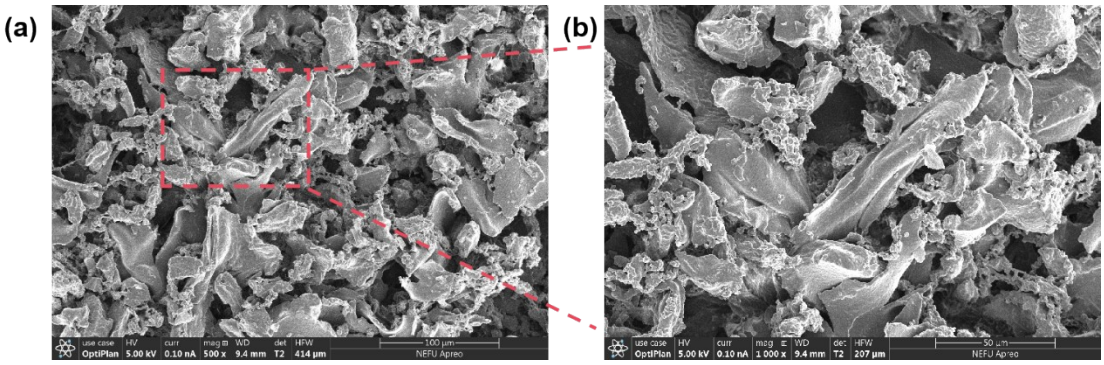

Figure S9 (a) SEM image of SEBS-5 film. (b) Partial magnification image of (a).

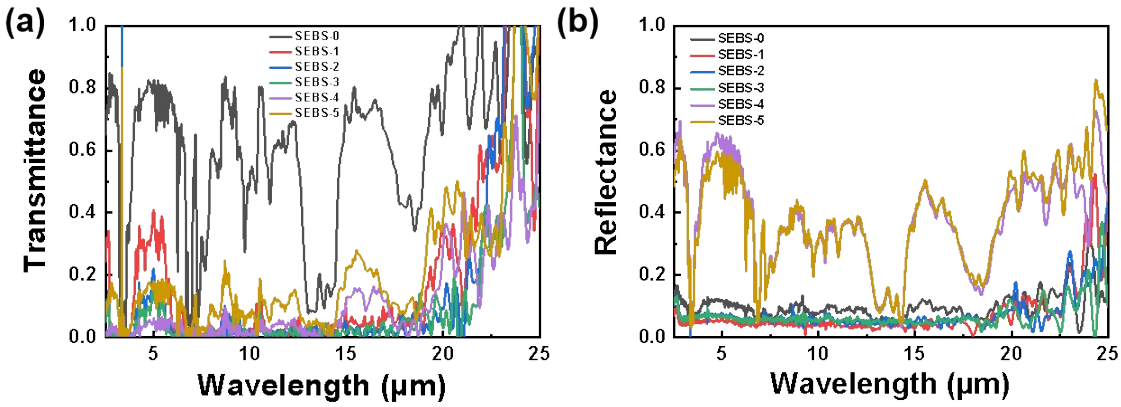

Figure S10 Reflectance spectra (a) and transmittance spectra (b) of SEBS-0, SEBS-1, SEBS-2, SEBS-3, SEBS-4, and SEBS-5 at the wavelength of 2.5-25 μm.

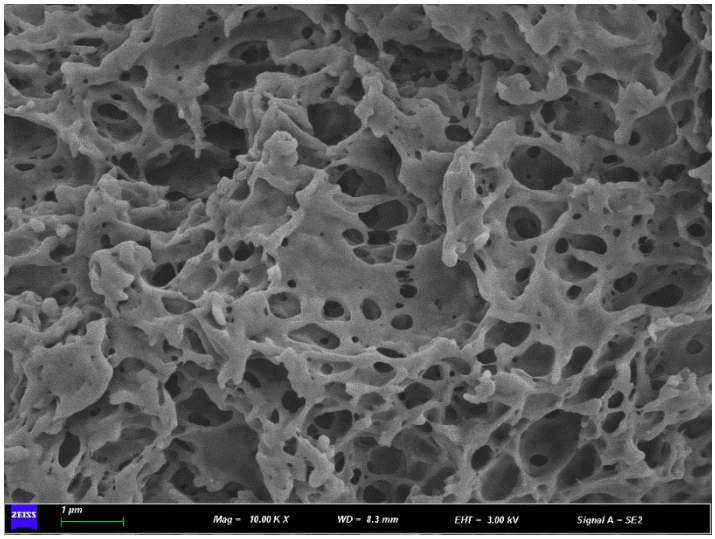

Figure S11 SEM image of EC powder.

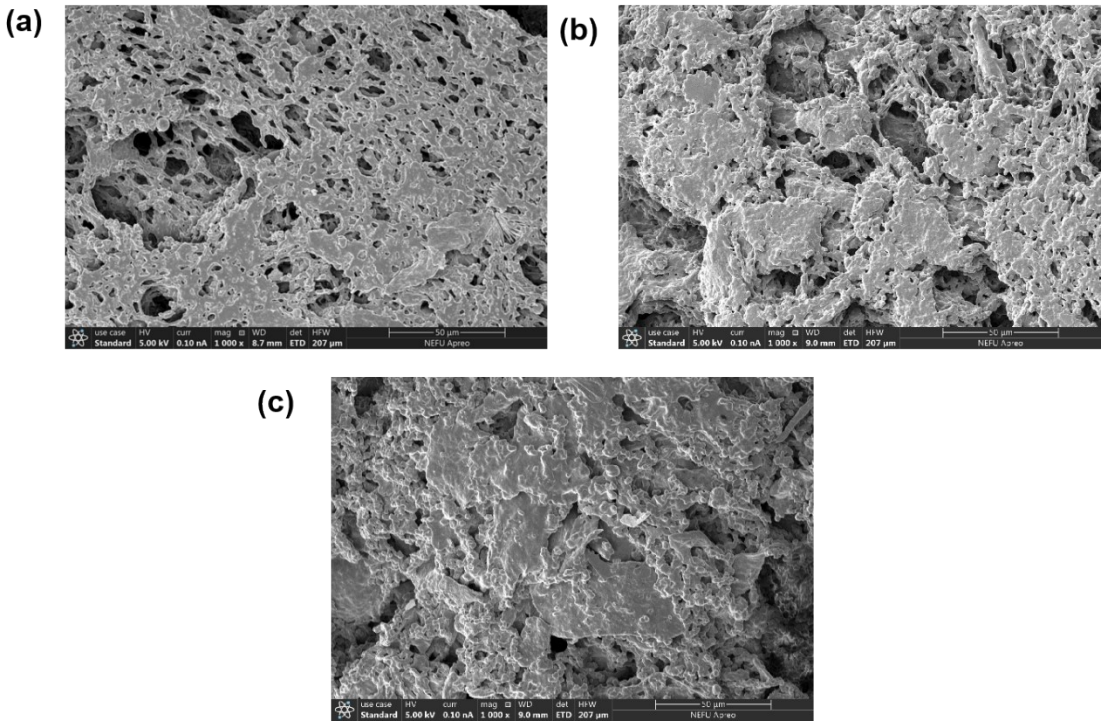

Figure S12 SEM images of (a)SEBS-EC-1 film, (b) SEBS-EC-2 film, and (c) SEBS-EC-3 film.

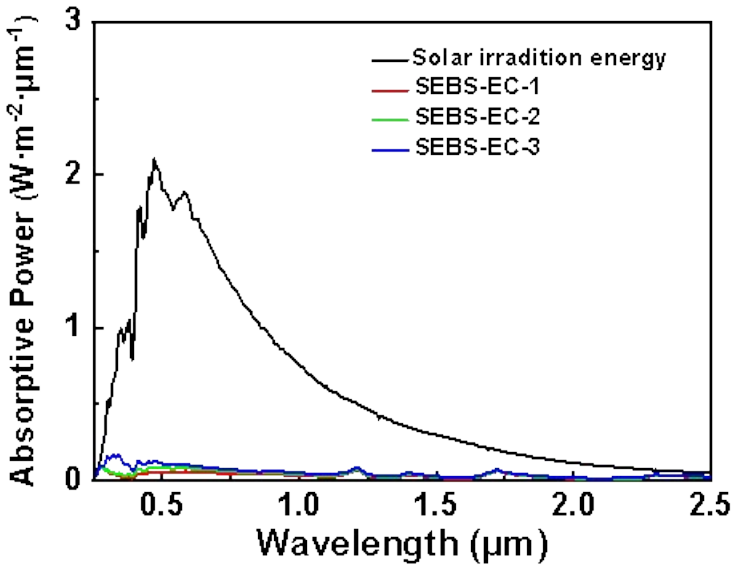

Figure S13 Absorptive power curves of SEBS-EC-1, SEBS-EC-2, and SEBS-EC-3 films.

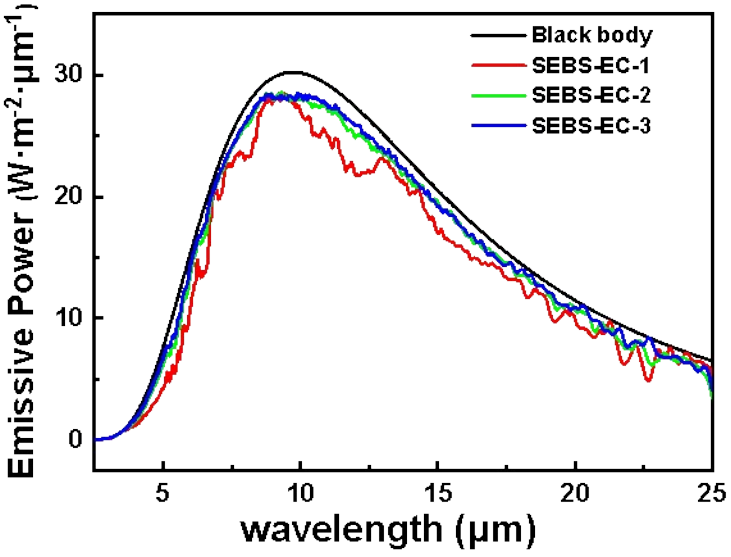

Figure S14 Emissive power curves of SEBS-EC-1, SEBS-EC-2, and SEBS-EC-3 films.

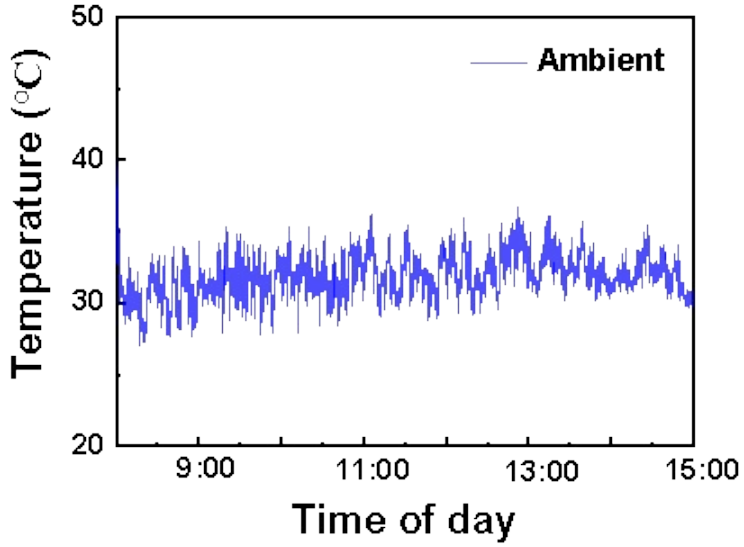

Figure S15 Ambient temperature of outdoor testing environment.

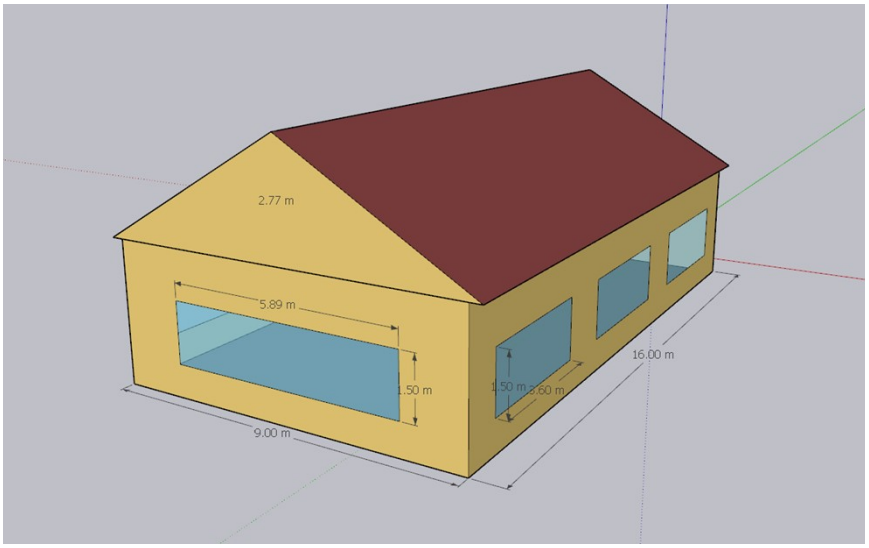

Figure S16 The building model for calculating the energy consumption per year.

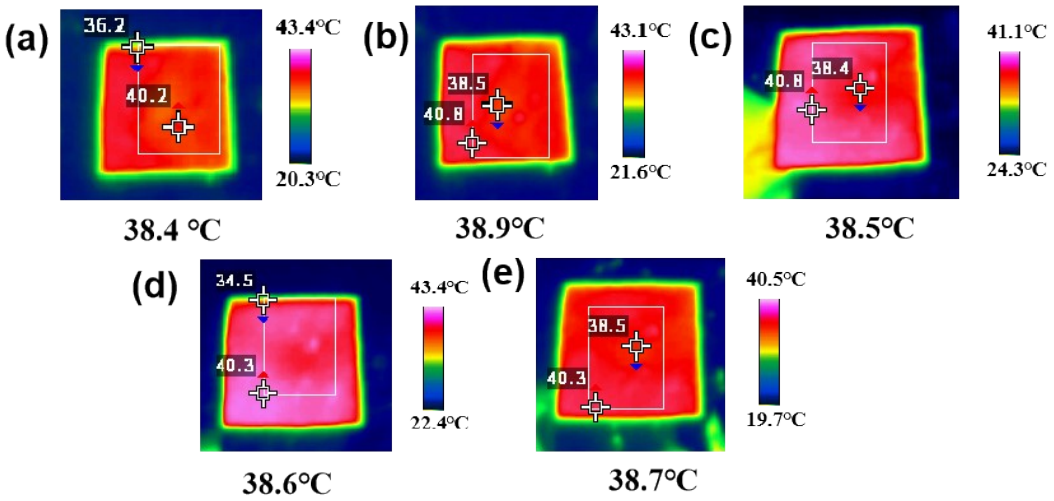

Figure S17 Infrared image of SEBS-EC film after UV exposure for (a) 48 h, (b) 96 h, (c) 144 h, (d) 192 h, and (e) 240 h.

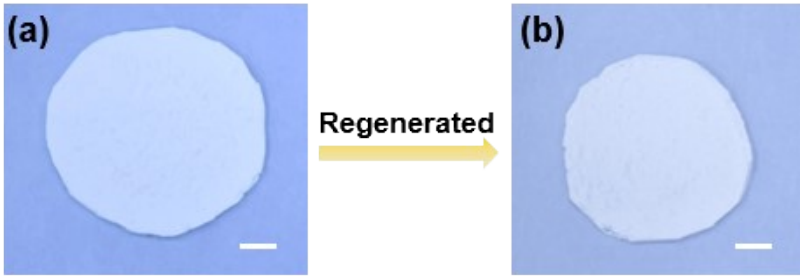

Figure S18 (a) Photograph of SEBS-EC film after UV exposure for 240 h. (b) Photograph of regenerated SEBS-EC film. (scale bar: 1 cm)

Table S1 A comparison of polymer-based PRC materials[1-18].

Materials	Preparation Method	R_{sol}	ε_{MIR}	P_{net} ($W \cdot m^{-2}$)	ΔT (℃)	UV durability	Ref.
SMB-PP	Melt-blown	~95%	0.82	-	4	-	[1]
Cellulose acetate (AC) thin film	Phase-separation	-	93.6%	47	5	-	[2]
Ethyl cellulose $BaSO_4$ coating	Brushing	98.6%	98.1%	-	2.5	-	[3]
Cellulose acetate/ TiO_2@PT composite film	Phase-separation	97.6%	0.95	-	6.5	R_{sol} of 97% after 720 h UV exposure	[4]
SAP-PRC coating	Surface modification	~97.58 %	~98%		7	-	[5]
Cellulose cooling paper	Hot-pressing	94%	0.95		8.8	-	[6]
Cellulose film	Electrostatic-field-assisted self-assembly	-	-	-	11.3	-	[7]
Cellulose Metamaterial	Scalable ball milling technology	~98	0.97	-	5.7	-	[8]
Cellulose nanocrystals (CNCs) based film	Evaporation-induced self-assembly	95.2%	96.5%	119	-	-	[9]
Bioinspired radiative cooling film	Photolithography and etching	~98%	96%	96.6	8.8	-	[10]
Self-cleaning polymer-based metamaterial	Photolithography and etching	-	0.98	97	6	-	[11]

Silanized BC-liquid crystal film	Freeze-drying	-	87.65%	-	-	-	[12]
PVDF-HFP film	Phase separation	97.7%	96.7%	-	5.4	-	[13]
Yolk-shell dielectric scatterers	Emulsion templated method	97.4%	96.9%	-	-	-	[14]
PDMS/PFPE	Mixing	94.0%	95.1%	62.94	11.5	-	[15]
skin-conformable electronic textile	Electrospinning	＞90%	97%	-	10.5	-	[16]
Polyethylene fibers	Melt extrusion	93.6%	93.9%	104.3	-	-	[17]
Biomass film	Phase separation	96.3%	95.4%	-	8.5	Maintains after UV exposure of 7 days	[18]
SEBS-EC film	Nonsolvent-induced phase separation	94%	0.95	141.3	10.6	R_{sol} of 92.3% after UV exposure for 240 h	This work

SMB-PP: Surface-modified melt-blown polypropylene
SAP-PRC coating: super-amphiphobic passive radiative cooling coating
PVDF-HFP: polyvinylidene fluoride-hexafluoropropylene
PDMS/PFPE: polydimethylsiloxane/perfluoropolyether

Table S2 Chromatic value of SEBS-EC film after UV exposure.

Samples	L*	a*	b*
SEBS-0h	94.40	0.03	-0.31
SEBS-48h	94.60	0.02	-0.32
SEBS-96h	94.57	0.03	-0.31
SEBS-144h	94.23	0.04	-0.35
SEBS-196h	94.24	0.03	-0.36
SEBS-240h	94.31	0.03	-0.37

Reference

1. Z. Yang, J. Zhang, Bioinspired radiative cooling structure with randomly stacked fibers for efficient all-day passive cooling. *ACS Appl. Mater. Interfaces* **13**, 43387-43395 (2021).

2. J. Jaramillo-Fernandez, H. Yang, L. Schertel, G. L. Whitworth, P. D. Garcia, S. Vignolini, C. M. Sotomayor-Torres, Highly-scattering cellulose-based films for radiative cooling. *Adv. Sci.* **9**, 2104758 (2022).

3. R. Liu, Z. Zhou, X. Mo, P. Liu, B. Hu, J. Duan, J. Zhou, Green-manufactured and recyclable coatings for subambient daytime radiative cooling. *ACS Appl. Mater. Interfaces* **14**, 46972-46979 (2022).

4. C. Cai, F. Chen, Z. Wei, C. Ding, Y. Chen, Y. Wang, Y. Fu, Large scalable, anti-ultraviolet, strong cellulose film with well-defined dual-pores for longtime daytime radiative cooling. *Chem. Eng. J.* **476**, 146668 (2023).

5. S. Feng, L. Yao, M. Feng, H. Cai, X. He, X. Bu, Y. Huang, Y. Zhou, M. He, Superamphiphobic interface-enhanced inorganic coating for multi-environments tolerant and zero-energy building radiative cooling. *Chem. Eng. J.* **475**, 146191 (2023).

6. H. Sun, F. Tang, Q. Chen, L. Xia, C. Guo, H. Liu, X. Zhao, D. Zhao, L. Huang, J. Li, L. Chen, A recyclable, up-scalable and eco-friendly radiative cooling material for all-day sub-ambient comfort. *Chem. Eng. J.* **455**, 139786 (2023).

7. S. Zhong, J. Zhang, S. Yuan, T. Xu, X. Zhang, L. Xu, T. Zuo, Y. Cai, L. Yi, Self-assembling hierarchical flexible cellulose films assisted by electrostatic field for passive daytime radiative cooling. *Chem. Eng. J.* **451**, 138558 (2023).

8. C. Cai, X. Wu, F. Cheng, C. Ding, Z. Wei, X. Wang, Y. Fu, Cellulose metamaterials with hetero-profiled topology via structure rearrangement during ball milling for daytime radiative cooling. *Adv. Funct. Mater.*, **34,** 2405903 (2024).

9. K. Feng, L. Zhang, Y. Liu, K. Hu, Z. Ma, X. Pei, Y. Wu, F. Zhou, Iridescent transparent passive radiative cooling enabled by cellulose nanocrystal assemblies. *Chem. Eng. J.* **488**, 151176 (2024).

10. J. He, Q. Zhang, Y. Zhou, Y. Chen, H. Ge, S. Tang, bioinspired polymer films

with surface ordered pyramid arrays and 3D hierarchical pores for enhanced passive radiative cooling. *ACS Nano* **18**, 11120-11129 (2024).

11. G. Huang, A. R. Yengannagari, K. Matsumori, P. Patel, A. Datla, K. Trindade, E. Amarsanaa, T. Zhao, U. Köhler, D. Busko, B. S. Richards, Radiative cooling and indoor light management enabled by a transparent and self-cleaning polymer-based metamaterial. *Nat. Commun.* **15**, 3798 (2024).

12. B. Li, C. Valenzuela, Y. Liu, X. Zhang, Y. Yang, Y. Chen, L. Wang, W. Feng, Free-standing bacterial cellulose-templated radiative cooling liquid crystal films with self-adaptive solar transmittance modulation. *Adv. Funct. Mater.* **34**, 2402124 (2024).

13. L. Li, G. Liu, Q. Zhang, H. Zhao, R. Shi, C. Wang, Z. Li, B. Zhou, Y. Zhang, Porous structure of polymer films optimized by rationally tuning phase separation for passive all-day radiative cooling. *ACS Appl. Mater. Interfaces* **16**, 6504-6512 (2024).

14. P. Li, Y. Liu, X. Liu, A. Wang, W. Liu, N. Yi, Q. Kang, M. He, Z. Pei, J. Chen, P. Jiang, W. Li, H. Bao, X. Huang, Reversed yolk-shell dielectric scatterers for advanced radiative cooling. *Adv. Funct. Mater.* **34**, 2315658 (2024).

15. S. Li, G. Du, M. Pan, X. Wang, X. Dong, T. Huang, D. Hu, T. Ren, X. Li, H. Chen, X. Mai, Scalable and sustainable hierarchical-morphology coatings for passive daytime radiative cooling. *Adv. Compos. Hybrid Mater.* **7**, 15 (2024).

16. Y. Peng, J. Dong, Y. Zhang, Y. Zhang, J. Long, J. Sun, T. Liu, Y. Huang, Thermally comfortable epidermal bioelectrodes based on ultrastretchable and passive radiative cooling e-textiles. *Nano Energy* **120**, 109143 (2024).

17. M. Sun, F. Peng, S. Xu, X. Liu, K. Dai, G. Zheng, C. Liu, C. Shen, Polyethylene fibers containing directional microchannels for passive radiative cooling. *Mater. Horiz.* **11**, 1787-1796 (2024).

18. Z. W. Zeng, B. Tang, F. R. Zeng, H. Chen, S. Q. Chen, B. W. Liu, Y. Z. Wang, H. B. Zhao, An intelligent, recyclable, biomass film for adaptive day-night and year-round energy savings. *Adv. Funct. Mater.* **34**, 2403061 (2024).